Fiber-Optic Anemometer Based on Bragg Grating Inscribed in Metal-Filled Microstructured Optical Fiber

Jie Wang, Zheng-Yong Liu, Shaorui Gao, A. Ping Zhang, Yong-Hang Shen, and Hwa-Yaw Tam

***Abstract*—A compact all-fiber optical anemometer based on a fiber Bragg grating (FBG) inscribed in a metal-filled microstructured optical fiber (MOF) is presented. Six-hole MOF (SHMOF) with a suspended core is fabricated to engineer the evanescent field of the fundamental guided mode, and low-melting-point alloy is filled in the micro-holes to achieve highly efficient light-heat conversion. Such a metal-filled SHMOF can strongly absorb pumping light at 1450 nm to generate heat and forms a fiber-optic "hot wire". The Bragg grating at 850 nm is inscribed in the core of SHMOF and acts as an in-fiber sensor for monitoring wind-speed dependent temperature of the "hot wire". Experimental results show the sensitivity of the fiber-optic anemometer is as high as ~0.091 nm/(m/s) at wind speed of around 2 m/s. Such a compact anemometer is promising as a low-power-consumption optical flow-meter for remote sensing and on-chip integration.**

***Index Terms*—Fiber gratings, microstructured optical fibers, optical fiber devices, optical fiber sensors.**

I. Introduction

Precise measurement of fluid flow has drawn tremendous attention owing to its important applications in chemical engineering, energy and aerospace industry. A number of approaches have been demonstrated to develop flow sensors including monitoring time of flight [1], differential pressure measurement [2], and heat transfer [3], [4]. In recent years, fiber-optic flow sensors have attracted remarkable research interests because of their intrinsic advantages, such as electromagnetic interference immunity, resistance to corrosive environments, and multiplexing capability. A fiber Bragg grating (FBG) inscribed in a cobalt-doped fiber has been demonstrated as a fiber-optic thermal anemometer for remote air-flow monitoring [5]. Optical pumping power of several hundred milliwatts was typically used to optically heat the FBG based anemometer to reach desirable operation temperature. An alternative approach to develop fiber-optic "hot-wire" is to use metal-coated optical fiber. It has been demonstrated that metallic film coated fiber devices can be employed to obtain energy-efficient anemometers [6]–[8]. However, direct exposure of metallic coatings to surrounding environment is detrimental to fatigue endurance of the fiber devices. Therefore, those fiber devices have to be carefully packaged for applications in harsh conditions.

One of promising solutions to above limitations is the microstructured optical fiber (MOF) technology. MOFs with air holes in the cladding region have become a diversified platform for development of novel sensors, e.g. gas sensors [10], [11], biosensors [12], and refractive-index sensors [13], and functional devices, e.g. active photonic modulator [16]–[18] and thermal poling [19]. In this paper, we propose a novel fiber-optic anemometer based on a metal-filled MOF device. As shown in Fig. 1, a home-made six-hole MOF (SHMOF) with a photosensitive suspended core will be designed for FBG fabrication. Metal is then infiltrated into the surrounding micro-holes and acts as a light-heat conversion element in an enclosed environment. Compared with the previously demonstrated fiber-optic "hot-wire" anemometers, this device has advantages of both high light-heat conversion efficiency and good corrosion

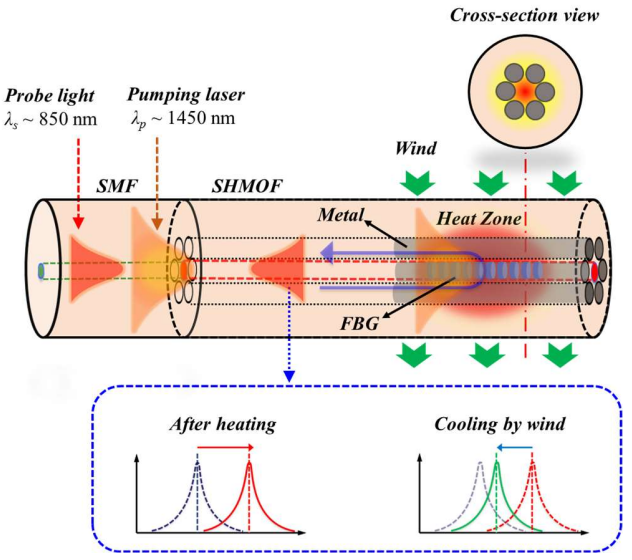

Fig. 1. Schematic diagram of the metal-filled SHMOF based anemometer. The inset at the bottom shows the spectral evolution of the FBG induced by laser heating and wind cooling.

This work was supported in part by Hong Kong RGC GRF (Grant No.: PolyU5246/13E).

J. Wang, Z. Y. Liu, S. R. Gao, A. P. Zhang, and H. Y. Tam are with the Department of Electrical Engineering, The Hong Kong Polytechnic University, Kowloon, Hong Kong, China (e-mail: azhang@polyu.edu.hk; eehytam@polyu.edu.hk).

J. Wang and Y. H. Shen are with the College of Optical Science and Engineering, Zhejiang University, Hangzhou 310027, China (e-mail: physyh@zju.edu.cn).

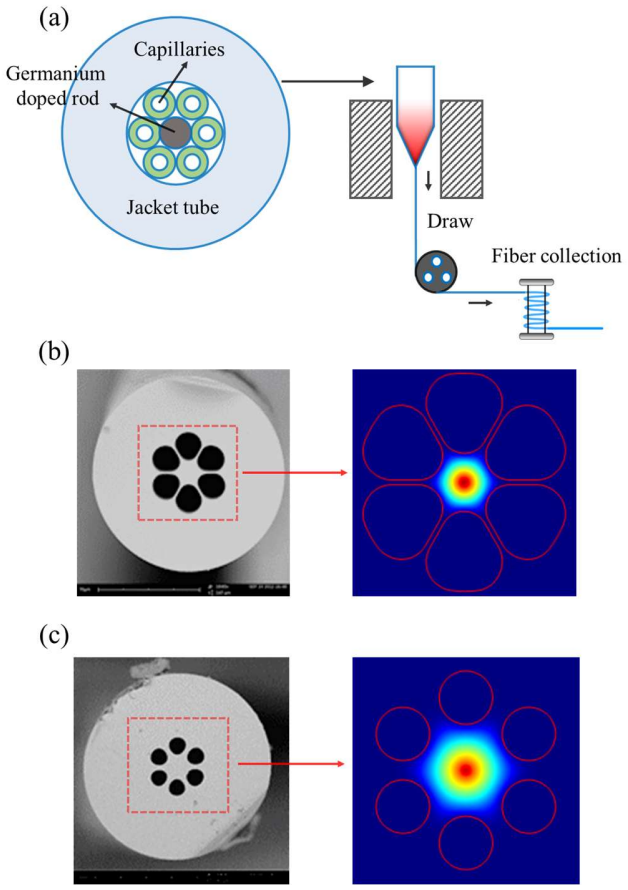

Fig. 2. (a) Schematic diagram of drawing procedure of the SHMOFs and SEM photos and corresponding modal profiles of the drawn (b) SHMOF-1 and (c) SHMOF-2 at 1450 nm.

resistance. Moreover, the design flexibility of the MOF (e.g. the diameters, pitches and configuration of micro-holes) offers an opportunity to improve its sensing performances, such as energy efficiency and multiplexing capability.

II. Fabrication and Modal Analysis of SHMOFs

The SHMOFs were home fabricated by using the stack-and-draw technique [22]. Fig. 2 (a) depicts the stacked preform in which six capillaries are regularly arranged in a hexagonal pattern and a Germanium doped rod is inserted in the center. In the experiment, two types of capillaries with different inner diameters were used to fabricate two kinds of SHMOFs with different modal properties. A jacket tube with outer and inner diameter (OD/ID) of 12 and 4 mm was used to hold the stacked matrix. During the drawing process, the pressure of ~40 kPa was applied to collapse small air gaps in the stacked preform. The drawing temperature and applied force were ~1960 ℃ and ~0.5 N, respectively.

The SEM photos of the fabricated SHMOFs were shown in Fig. 2(b) and (c). One can see that six air holes are regularly arranged in both SHMOFs. The air-holes of the first SHMOF (i.e. SHMOF-1), as shown in Fig. 2(b), are with the diameter of 17 μm and pitch of 18 μm, while the air-holes of the second SHMOF (i.e. SHMOF-2), as shown in Fig. 2(c), are with the diameter of 11 μm and pitch of 15 μm. The

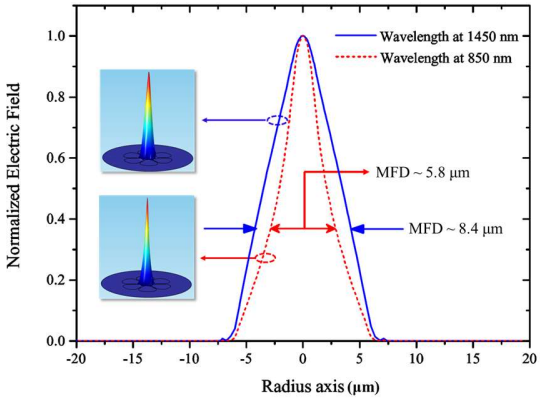

Fig. 3. Fundamental modal distribution of SHMOF-1 at 1450 (blue curve) and 850 nm (red curve), respectively. The insets show corresponding 3-D modal profiles.

big air-holes in both SHMOFs facilitate metal infiltration. The outer diameters of both SHMOFs are ~125 μm. A suspended germanium-doped core with diameter of 2 μm was fabricated in both SHMOFs to support modal guidance and grating inscription.

Modal properties of both SHMOFs were simulated with the finite element method (FEM). The micro-holes are assumed to be filled with air in the simulation. As shown in Fig. 2(b) and (c), SHMOF-1 exhibits stronger light confinement than SHMOF-2 as expected.

Modal properties of SHMOF-1 at wavelengths of 850 and 1450 nm are compared in Fig. 3. The fundamental modal field diameter (MFD) at 850 nm is calculated as ~5.8 μm, which is smaller than that at 1450 nm, i.e. ~8.4 μm. It means that propagation loss induced by metal filled in the air-holes at 850 nm is much lower than that at 1450 nm. Therefore, we will use an FBG with a reflection peak at 850 nm for monitoring temperature, whereas a pump laser at the wavelength of 1450 nm will be used to optically heat the FBG in the experiment.

III. Grating Inscription and Metal Filling in SHMOFs

After soaked in hydrogen at ~15 bar and room temperature for two days, the SHMOFs (i.e. SHMOF-1 and SHMOF-2) were used to inscribe FBGs with the central wavelength of ~850 nm. Fig. 4(a) illustrates the schematic diagram of the phase mask based setup used to fabricate FBGs in the SHMOFs. The pitch of the phase mask is 584.1 nm. After inscription of FBGs, the resulted SHMOFs were then used for infiltration of low-melting-point alloy (Bi-Sn-In). Fig. 4(b) shows the schematic diagram of the metal infiltration setup used in the experiments. The SHMOF was inserted into a well-sealed heat chamber. One fiber end was immersed in a container filled with solid alloy particles, while the other end was left open outside of the chamber. After heated at the temperature of 175°C for around half an hour, the melted alloy in liquid phase was forced into the six micro-holes by nitrogen gas under the pressure of ~3 bar. The total length of the SHMOF filled with alloy was about 11

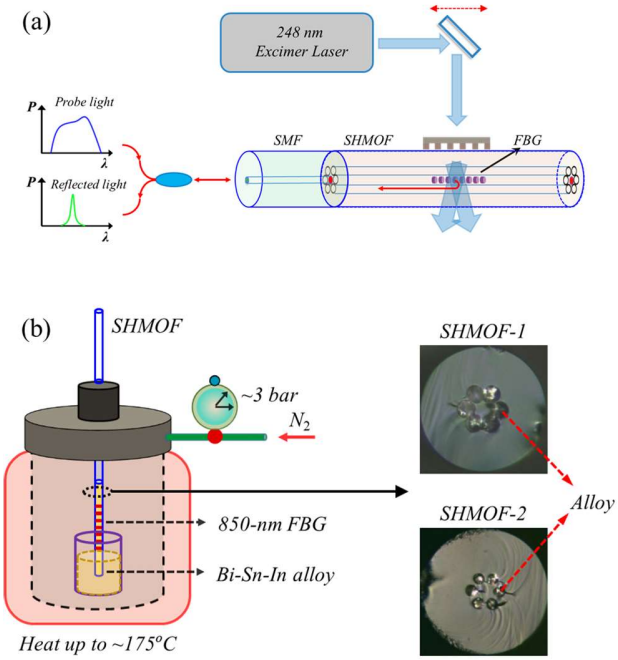

Fig. 4. Schematic diagram of (a) FBG fabrication and (b) metal infiltration in the SHMOFs. The insets show the corresponding cross-sectional microscope images of SHMOF-1 (upper-right) and SHMOF-2 (bottom-right) filled with alloy, respectively.

cm, which is mainly limited by the height of the heat chamber. The metal infiltration results were verified through inspecting the cross-sections of the processed fibers by using an optical microscope. Fig. 4(b) shows the cross-sections of the metal-filled SHMOF-1 and SHMOF-2. One can see that all six micro-holes were completely filled with alloy in both fibers. The cracks on those cross-sections were due to the non-optimized cleaving conditions.

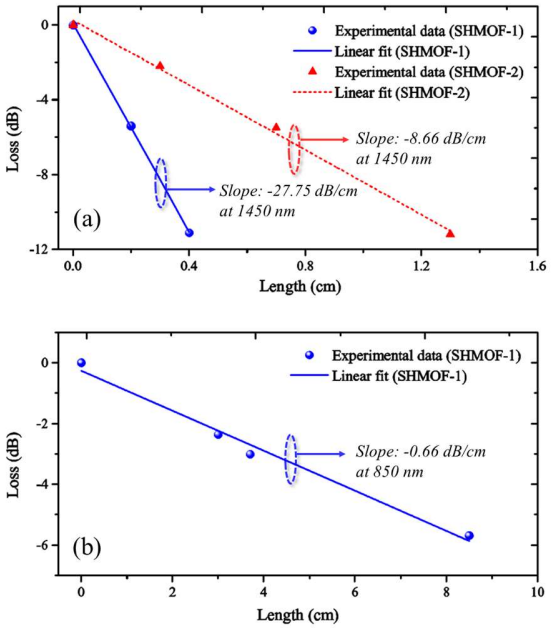

Fig. 5. Measured propagation losses of the metal-filled SHMOFs at the wavelength of (a) 1450 nm and (b) 850 nm, respectively.

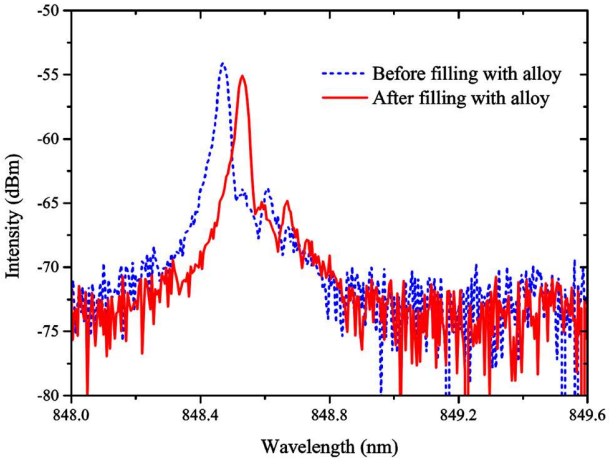

Fig. 6. Reflection spectrum of FBG before (blue dash curve) and after (red solid curve) alloy filling in the SHMOF-1.

The propagation losses of the fabricated metal-filled SHMOFs were then measured by using the cut-back method. Using a 0.4-cm long metal-filled SHMOF-1 and a 1.3-cm long metal-filled SHMOF-2, we obtained the loss of metal-filled SHMOF-1 as -27.75 dB/cm at 1450 nm, which is larger than that of metal-filled SHMOF-2, i.e. -8.66 dB/cm, as shown in Fig. 5 (a). The measurement result proves that the MOF technology can be used to tailor the absorption of pumping light through controlling the fiber microstructure parameters. A longer metal-filled SHMOF-1 with the length of 8.5 cm was used to measure its propagation loss at 850 nm. As shown in Fig. 5 (b), the measured loss of the metal-filled SHMOF-1 at the wavelength of 850 nm is as low as -0.66

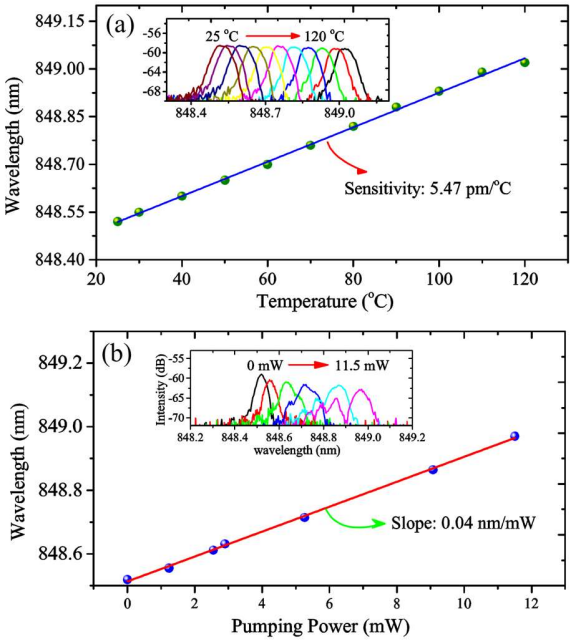

Fig. 7. Bragg wavelengths of the FBG inscribed in the metal-filled SHMOF-1 as a function of (a) temperature and (b) launched pumping power. The insets show the corresponding Bragg spectral evolution.

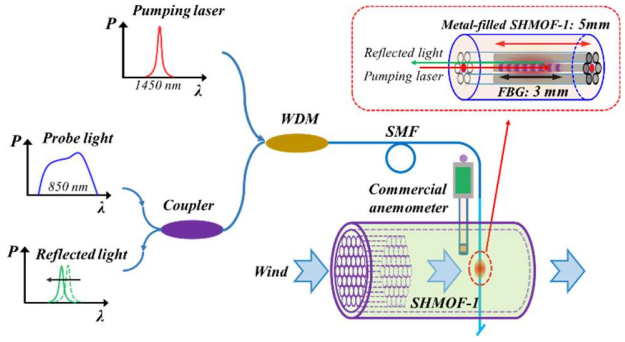

Fig. 8. Schematic diagram of the setup for testing FBG anemometers.

dB/cm. It confirms that the light wave at a shorter wavelength is a better choice as the probe signal of such a fiber sensor.

Fig. 6 shows the difference of the reflection spectra of the FBG written in SHMOF-1 before and after infiltrating with alloy. Due to the increment of the effective refractive index after metal infusion, its Bragg wavelength red-shifts by ~0.06 nm. The power of the reflection peak dropped ~1 dB mainly because of the metal-induced loss. The thermal response of the FBG was measured by heating fiber in a furnace at the temperature between 25 and 120 °C. The spectral evolution of the FBG against temperature was recorded as shown in Fig. 7(a). The measured thermal sensitivity is 5.47 pm/°C.

The response of the FBG to the launched pumping laser at 1450 nm was also measured in the experiment. As shown in Fig. 7(b), the Bragg wavelength increases with pumping power with the slope of 0.04 nm/mW. The reflection spectrum was observed to be broadened at higher pumping power, which is resulted from the temperature gradient induced chirp of the FBG. Nevertheless, the reflection peak is still well discriminable. The measured optically heating efficiency of the presented "hot-wire" is ~7.3 °C/mW.

IV. Measurement Results of Anemometer

The optical fiber anemometer, which was fabricated by using a 3-mm long FBG inscribed in a 5-mm long metal-filled SHMOF-1, was then tested by using a small wind tunnel at room temperature. Fig. 8 illustrates the wind-speed measurement setup. The wind direction was perpendicular to the installed fiber. A commercial electric anemometer was installed nearby the FBG sensor as a measurement reference. A broadband light source with the output power of ~5 mW at the wavelength of ~850 nm and an optical spectrum analyzer (OSA) were used to monitor the FBG spectral response with respect to wind speed. The pumping light at the wavelength of ~1450 nm was launched into the metal-filled SHMOF-1 through a wavelength-division multiplexer (WDM).

In the measurement, the FBG written in the SHMOF-1 was initially heated by the pumping laser. Once the FBG was blown by the wind, it was cooled down which induced a blue shift of its peak wavelength. Based on the theory of hot-wire

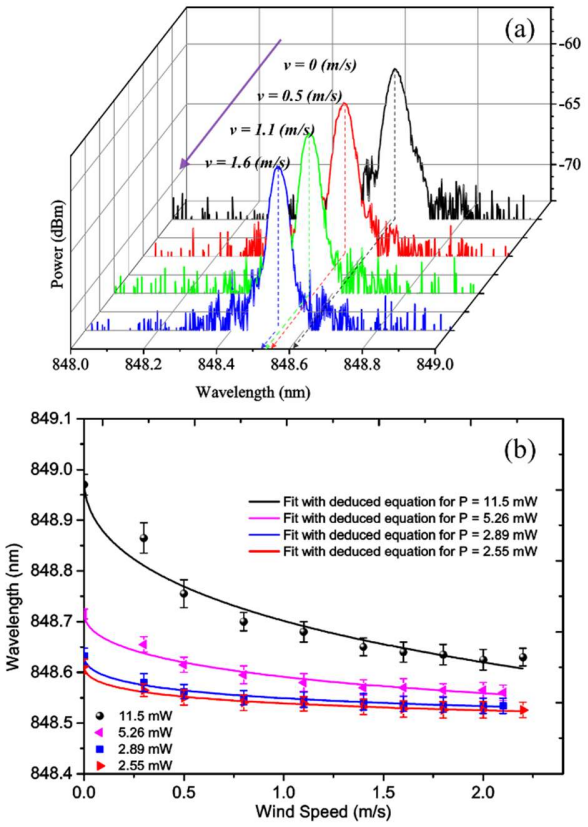

Fig. 9. (a) Spectral evolution of the anemometer against wind speed under pumping power of 2.55 mW and (b) Wavelength shifts with respect to the wind speeds under the pumping powers of 11.5 mW, 5.26 mW, 2.89 mW and 2.55 mW, respectively.

anemometry [23], the relationship between the heat loss, H_{loss}, and the wind speed, v, is known as

$$H_{loss} = \Delta T \cdot (A + B\sqrt{v}), \quad (1)$$

where ΔT is the temperature difference between the optically-heated SHMOF and ambient environment, v is the wind

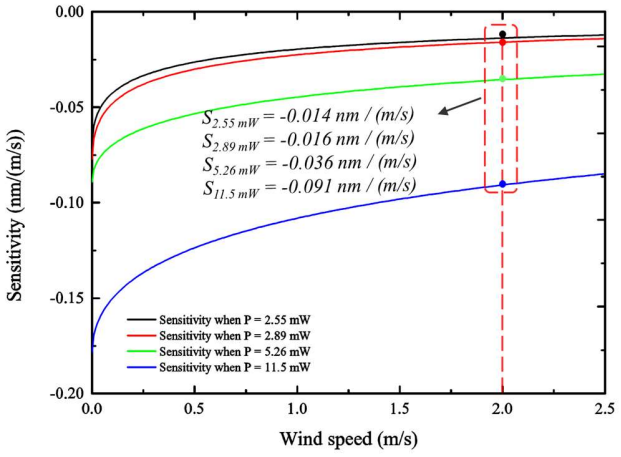

Fig. 10. Sensitivity as a function of wind speed under different pumping powers of P = 2.55, 2.89, 5.26, and 11.5 mW.

speed, and A, B are empirical calibration constants. According to the law of energy conservation, the heat loss H_{loss} equals to the light-power consumption of the anemometer. On the other hand, the dependence of the Bragg wavelength shift, $\Delta\lambda$, on the temperature change, ΔT, is well known as [24]

$$\Delta\lambda = 2n_{eff}\Lambda(\alpha+\xi)\Delta T\ , \tag{2}$$

where n_{eff} is the effective index of fundamental mode at ~850 nm in the metal-filled SHMOF, Λ is the grating pitch, α is the thermal expansion coefficient and ξ is the thermo-optic coefficient of the silica fiber. Thus, the instant Bragg wavelength can be expressed as a function of wind speed as

$$\lambda_B = \lambda_0 + 2n_{eff}\Lambda(\alpha+\xi)\cdot H_{loss}\ /(A+B\sqrt{v})\,. \tag{3}$$

where λ_B and λ_0 are the instant and initial Bragg wavelength of the FBG, respectively.

Figure 9 shows the experimental results of the anemometric test. Fig. 9(a) shows the response of the sensor when pumping power was set to 2.55 mW and the wind speed is gradually increased from 0 to 1.6 m/s. Fig. 9(b) shows the dependences of the FBG's peak wavelength on wind speeds when pumping powers of 2.55, 2.89, 5.26, and 11.5 mW were applied to optically heat the FBG sensor. The solid curves are fitted by using Eq. 3. One can see that the fitted curves of experimental results are consistent with the theoretical formula. The causes of the measurement deviation indicated by error bars ought to be the relatively low resolution of the OSA and the measurement error of the commercial anemometer. In general, the responses of the FBG anemometer in the full wind-speed range are nonlinear as other reported results [5]. If the first derivatives of the fitted curves are used to estimate the sensitivity, as shown in Fig. 10, the sensitivities at wind speed v = 2 m/s are 0.014, 0.016, 0.036 and 0.091 nm/(m/s) for pumping powers of 2.55, 2.89, 5.26 and 11.5 mW, respectively. The highest sensitivity is close to that reported in [5], but the required pumping power (i.e. 11.5 mW) is one order of magnitude lower. If an FBG interrogator with the resolution of 1 pm is used for signal interrogation, the sensor's measurement resolutions of wind speed can be estimated as 0.072, 0.063, 0.028 and 0.011 m/s under corresponding pumping powers, respectively.

V. Conclusion

In conclusion, a low-power-consumption fiber-optic anemometer based on an FBG inscribed in a metal-filled MOF has been demonstrated. Specially designed SHMOFs have been fabricated for FBG inscription and metal infiltration. The developed anemometer exhibits very efficient light-heat conversion, and a sensitivity of ~0.091 nm/(m/s) has been demonstrated by using a very low pumping power of ~11.5 mW. Such a miniature energy-efficient fiber-optic flow sensor is promising for remote flow monitoring and on-chip sensing.

References

[1] J. Wu and W. Sansen, "Electrochemical time of flight flow sensor," Sensors Actuators, A Phys., vol. 97–98, no. October 2001, pp. 68–74, 2002.

[2] N. Svedin, E. Kalvesten, and G. Stemme, "A new edge-detected lift force flow sensor," J. Microelectromechanical Syst., vol. 12, no. 3, pp. 344–354, 2003.

[3] S. Oda, M. Anzai, S. Uematsu, and K. Watanabe, "A silicon micromachined flow sensor using thermopiles for heat transfer measurements," IEEE Trans. Instrum. Meas., vol. 52, no. 4, pp. 1155–1159, 2003.

[4] M. Domínguez, F. N. Masana, V. Jiménez, S. Bermejo, J. Amirola, J. Ballester, N. Fueyo, and L. M. Castañer, "Low-cost thermal Σ-Δ air flow sensor," IEEE Sens. J., vol. 2, no. 5, pp. 453–462, 2002.

[5] S. Gao, A. P. Zhang, H.-Y. Tam, L. H. Cho, and C. Lu, "All-optical fiber anemometer based on laser heated fiber Bragg gratings," Opt. Express, vol. 19, no. 11, pp. 10124–10130, 2011.

[6] L. J. Cashdollar and K. P. Chen, "Fiber Bragg grating flow sensors powered by in-fiber light," Sensors Journal, IEEE, vol. 5, no. 6, pp. 1327–1331, 2005.

[7] X. Dong, Y. Zhou, W. Zhou, J. Cheng, and Z. Su, "Compact anemometer using silver-coated fiber Bragg grating," IEEE Photonics J., vol. 4, no. 5, pp. 1381–1386, 2012.

[8] P. Caldas, P. A. S. Jorge, G. Rego, O. Frazão, J. L. Santos, L. A. Ferreira, and F. Araújo, "Fiber optic hot-wire flowmeter based on a metallic coated hybrid long period grating/fiber Bragg grating structure," Appl. Opt., vol. 50, no. 17, pp. 2738–2743, 2011.

[9] B. Eggleton, C. Kerbage, P. Westbrook, R. Windeler, and A. Hale, "Microstructured optical fiber devices," Opt. Express, vol. 9, no. 13, pp. 698–713, 2001.

[10] Y. L. Hoo, W. Jin, C. Shi, H. L. Ho, D. N. Wang, and S. C. Ruan, "Design and modeling of a photonic crystal fiber gas sensor," Appl. Opt., vol. 42, no. 18, pp. 3509–3515, 2003.

[11] Y. Guofeng, A. P. Zhang, M. Guiying, W. Binhao, K. Bongkyun, I. Jooeun, H. Sailing, and C. Youngjoo, "Fiber-Optic Acetylene Gas Sensor Based on Microstructured Optical Fiber Bragg Gratings," Photonics Technol. Lett. IEEE, vol. 23, no. 21, pp. 1588–1590, 2011.

[12] T. M. Monro, S. Warren-Smith, E. P. Schartner, A. François, S. Heng, H. Ebendorff-Heidepriem, and S. Afshar V, "Sensing with suspended-core optical fibers," Opt. Fiber Technol., vol. 16, no. 6, pp. 343–356, 2010.

[13] A. P. Zhang, G. Yan, S. Gao, S. He, B. Kim, J. Im, and Y. Chung, "Microfluidic refractive-index sensors based on small-hole microstructured optical fiber Bragg gratings," Appl. Phys. Lett., vol. 98, no. 22, p. 221109, 2011.

[14] T. Larsen, A. Bjarklev, D. Hermann, and J. Broeng, "Optical devices based on liquid crystal photonic bandgap fibres.," Opt. Express, vol. 11, no. 20, pp. 2589–2596, 2003.

[15] P. Zu, C. Chiu Chan, T. Gong, Y. Jin, W. Chang Wong, and X. Dong, "Magneto-optical fiber sensor based on bandgap effect of photonic crystal fiber infiltrated with magnetic fluid," Appl. Phys. Lett., vol. 101, no. 24, p. 241118, 2012.

[16] M. Fokine, L. E. Nilsson, Ã. Claesson, D. Berlemont, L. Kjellberg, L. Krummenacher, and W. Margulis, "Integrated fiber Mach-Zehnder interferometer for electro-optic switching," Opt. Lett., vol. 27, no. 18, pp. 1643–1645, 2002.

[17] G. Chesini, C. M. B. Cordeiro, C. J. S. de Matos, M. Fokine, I. C. S. Carvalho, and J. C. Knight, "All-fiber devices based on photonic crystal fibers with integrated electrodes.," Opt. Express, vol. 17, no. 3, pp. 1660–1665, 2009.

[18] N. Myren and W. Margulis, "All-fiber electrooptical mode-locking and tuning," Photonics Technol. Lett. IEEE, vol. 17, no. 10, pp. 2047–2049, 2005.

[19] N. Myrén, H. Olsson, L. Norin, N. Sjödin, P. Helander, J. Svennebrink, and W. Margulis, "Wide wedge-shaped depletion region in thermally poled fiber with alloy electrodes.," Opt. Express, vol. 12, no. 25, pp. 6093–6099, 2004.

[20] S. H. Lee, B. H. Kim, and W.-T. Han, "Effect of filler metals on the temperature sensitivity of side-hole fiber.," Opt. Express, vol. 17, no. 12, pp. 9712–9717, 2009.

[21] Z. Yu, W. Margulis, O. Tarasenko, H. Knape, and P. Y. Fonjallaz, "Nanosecond switching of fiber Bragg gratings," Opt. Express, vol. 15, no. 22, pp. 14948–14953, 2007.

[22] Z. Liu, C. Wu, M. L. V. Tse, and H. Y. Tam, "Fabrication, characterization, and sensing applications of a high-birefringence suspended-core fiber," J. Light. Technol., vol. 32, no. 11, pp. 2113–2122, 2014.

[23] H. H. Brunn, Hot-wire Anemometry: Principles and Signal Analysis. Oxford University Press, 1995.

[24] A. Kersey, M. A. Davis, H. J. Patrick, M. Leblanc, K. P. Koo, C. G. Askins, M. A. Putnam, and E. J. Friebele, “Fiber grating sensors,” Light. Technol. J., vol. 15, no. 8, pp. 1442–1463, 1997.